IOPscience iopscience.iop.org

Home Search Collections Journals About Contact us My IOPscience

Symmetric Daubechies' wavelets and numerical solution of NLS equations

This article has been downloaded from IOPscience. Please scroll down to see the full text article.

1994 J. Phys. A: Math. Gen. 27 8207

(http://iopscience.iop.org/0305-4470/27/24/027)

View the table of contents for this issue, or go to the journal homepage for more

Download details:
IP Address: 171.66.16.68
The article was downloaded on 01/06/2010 at 23:00

Please note that terms and conditions apply.

J. Phys. A: Math. Gen. 27 (1994) 8207–8230. Printed in the UK

Symmetric Daubechies' wavelets and numerical solution of NLS equations*

L Gagnon†§ and J M Lina†‡||

† Groupe PHYSNUM, Labo. de Phys. Nucl., Université de Montréal, CP 6128, Succ. Centre-Ville, Montréal, Québec, Canada H3C 3J7

‡ Atlantic Nuclear Services Ltd, Fredericton, New Brunswick, Canada E3B 5C8

Received 30 August 1994, in final form 19 October 1994

Abstract. Recent work has shown that wavelet-based numerical schemes are at least as effective and accurate as standard methods and may allow an 'easy' implementation of a spacetime adaptive grid. Up to now, wavelets which have been used for such studies are the 'classical' ones (real Daubechies' wavelets, splines, Shannon and Meyer wavelets, etc) and were applied to diffusion-type equations. The present work differs in two points. Firstly, for the first time we use a new set of complex symmetric wavelets which have been found recently. The advantage of this set is that, unlike classical wavelets, they are simultaneously orthogonal, compactly supported *and symmetric*. Secondly, we apply these wavelets to the physically meaningful cubic and quintic nonlinear Schrödinger equations. The most common method to simulate these models numerically is the symmetrized split-step Fourier method. For the first time, we propose and study a new way of implementing a global spacetime adaptive discretization in this numerical scheme, based on the interpolation properties of complex-symmetric scaling functions. Second, we propose a locally adaptive 'split-step wavelet' method.

1. Introduction

This paper is devoted to an application of complex-symmetric Daubechies' wavelets and scaling functions to numerical simulation of nonlinear partial differential equations (PDEs). The mathematical models we have retained are the cubic ($\sigma = 1$) and quintic ($\sigma = 2$) nonlinear Schrödinger (NLS) equations

$$iu_t + \tfrac{1}{2}u_{xx} + \lambda u|u|^{2\sigma} = 0 \qquad \lambda \in \mathbb{R}^* \tag{1.1}$$

because they can exhibit strong gradients for particular initial conditions and of their importance in nonlinear optics as well as in many other fields. Throughout this paper, we use t as the evolution parameter (which is a space variable in nonlinear optics) and the notation NLS'+' for $\lambda > 0$ and NLS'−' for $\lambda < 0$.

The idea of using wavelets to perform numerical simulations of PDEs is not new [1–8]. The motivation comes from the fact that wavelets provide a mathematical representation which can resolve numerical difficulties due to singular phenomena. More exactly, properties such as orthogonality and the compact support of multi-resolution bases (scaling

* This work is supported in part through funds provided by the Natural Sciences and Engineering Research Council (NSERC) of Canada.

§ E-mail address: lgagnon@lps.umontreal.ca

|| E-mail address: lina@lps.umontreal.ca

0305-4470/94/248207+24$19.50 © 1994 IOP Publishing Ltd

functions and wavelets) as well as the exact representation of polynomials of a fixed degree on scaling functions, allow efficient and stable calculation of regions with transient phenomena or strong oscillations. In addition, the multi-resolution structure of wavelet orthonormal bases can provide a simple and effective framework for spacetime adaptive algorithms; the adaptive-mesh refinement is implemented by successively adding layers of 'detail' which increase the resolution of the numerical approximation.

In previous work, numerical implementations of wavelets have been performed using two main approaches. A first one, known as the wavelet–Galerkin method, consists of projecting the solution of the PDE onto the space spanned by the integer translation of the scaling function [1–3, 6]. To have good approximation properties, orthogonality and compact support of the basis elements are required. The choice of the scaling function is also motivated by the regularity of the projection wanted, that is, the maximum degree of the polynomials contained in the projection space. For these reasons, Daubechies' scaling functions have been widely used in such analysis. Although the asymmetry of the real Daubechies' scaling functions does not seem to introduce a significant asymmetry in the numerical solution, we think that the use of symmetric scaling functions, as is the case in this work, should lead to even more accurate results. A second approach makes use of the multi-resolution properties of the wavelets in order to develop adaptive numerical schemes [4, 5, 7, 8]. Here, the projection is made onto the orthogonal wavelet spaces themselves, up to some scaling function space which fixes the coarsest resolution. The wavelet spaces are the 'details spaces' of the numerical approximation and contain informations at different resolution levels. The idea is to track the singularity by adding successive layers of resolution, that is, adding wavelets which are sensitive at finer scales. For better stability, the time-step of such numerical schemes can also be adapted [8].

Up to now, the wavelets which have been used for such studies are the 'classical' ones (real Daubechies' wavelets, splines, Shannon and Meyer wavelets, etc) and were applied to real-valued models: Burger, diffusion and linear advection equations. The Burger equation was the most popular 'laboratory' because (i) it constitutes, from a numerical point of view, a one-dimensional version of the important Navier–Stokes equation, (ii) it can develop sharp gradients in the small viscosity limit, and (iii) the exact solution of the Cauchy problem is known. For these models, wavelet-based numerical schemes have been shown to be at least as effective and accurate as standard methods [1, 8].

Our work differs in two respects. First, for the first time we use a new set of complex wavelets which have been found recently [9] using a particular parametrization of the multi-resolution analyses [10]. The advantage of this set is that, unlike classical wavelets, they are simultaneously orthogonal, compactly supported *and symmetric*. Second, we apply these wavelets to the cubic and quintic NLS equations (1.1), which are historically two of the most important models 'on the market' and have numerous applications in optics, fluid dynamics, engineering, biology, chemistry and applied mathematics [11–16]. The cubic NLS equation is also a limiting case of the Navier–Stokes equation and has an exact formulation of the Cauchy problem in terms of the inverse scattering method. In addition, both models can also lead to strong gradient phenomena. For the cubic NLS'$-$' model, smooth localized initial conditions can evolve toward a typical breaking-wave phenomena which exhibits very high-frequency oscillations [17, 18]. Also, the quintic NLS'$+$' equation, which has similar properties to the $(2+1)$-dimensional cubic NLS'$+$' equation which models the three-dimensional self-focusing theory in nonlinear optics, can generate solutions with localized structures in space which evolve quickly in time and eventually blow up [19–21]. Finally, the breather solutions [14, 22] (also known as the bounded N-soliton solutions) of

the cubic NLS'+' equations exhibit periodic peaking of the field and can be use to test the ability of an adaptive algorithm to increase *and decrease* the resolution.

This paper is organized as follows. In section 2, we recall the mathematical background needed to understand the paper: wavelet multi-resolution theory [23–26], complex-symmetric Daubechies wavelets [9], representation of differential operators, collocation techniques and wavelet transform. This is not a mere exercise since the subject is relatively new. In addition, we reformulate some known results in a simpler and original way. In section 3, we show how the split-step Fourier method [14,27,28] can be reformulated in terms of wavelet–Galerkin projection or multi-resolution analysis. We compare the accuracy of the Fourier and wavelet–Galerkin versions on the typical soliton propagation simulation. In section 4, we propose and study a new way of implementing a global spacetime adaptive discretization in the numerical scheme based on the recomposition properties of higher-order scaling functions. This globally adaptive algorithm will be tested on typical high-gradient simulations (optical breaking waves, wave-collapse and bound-soliton solutions). Here we are more concerned with the feasibility and accuracy of the algorithm rather than its simulation time efficiency. Finally, in section 5, we concentrate on a full wavelet decomposition. We give a description of a possible local spacetime adaptive scheme which implements the multi-resolution analysis and incorporates a global interpolation scheme using scaling functions in a pseudo-spectral way.

2. Mathematical backgrounds

2.1. Multi-resolution analysis

Let us first describe the basic idea and the principal characteristics of the multi-resolution wavelet decomposition. The main equation of the multi-resolution theory is the scaling equation which establishes a connection between the two symmetries underlying the wavelet theory: dilations and translations. Given a set of coefficients $a_k, k \in \mathbb{Z}$ which we will describe later on, the scaling equation

$$\varphi(x) = 2\sum_k a_k \varphi(2x - k) \qquad x \in \mathbb{R} \tag{2.1}$$

and the normalization

$$\int \varphi(x)\,\mathrm{d}x = \sum_k a_k = 1 \tag{2.2}$$

define a scaling function $\varphi(x)$. By defining the set of translates of the dilated function $\varphi(x)$,

$$\varphi_{j,k}(x) = 2^{j/2}\varphi\left(2^j x - k\right) \qquad j \in \mathbb{Z} \tag{2.3}$$

the multi-resolution analysis of $L^2(\mathbb{R})$ consists of the decomposition of the Hilbert space $L^2(\mathbb{R})$ (the space of square-integrable functions) into the chain of closed subspaces

$$\cdots \subset V_{j-1} \subset V_j \subset V_{j+1} \subset \cdots \tag{2.4}$$

where

$$V_j = \mathrm{Span}\,\{\varphi_{j,k}(x), k \in \mathbb{Z}\} \tag{2.5}$$

and such that

$$\bigcap_j V_j = \{0\} \qquad \bigcup_j V_j = L^2(\mathbb{R})\,. \tag{2.6}$$

Multi-resolution aims to decompose $L^2(\mathbb{R})$ as

$$L^2(\mathbb{R}) = V_{j_0} \oplus \sum_{j \geqslant j_0} W_j \tag{2.7}$$

where W_j is defined as the orthogonal complement of V_j in V_{j+1}, that is

$$V_{j+1} = V_j \oplus W_j\,. \tag{2.8}$$

For a given scale j,

$$W_j = \text{Span}\,\{\psi_{j,k}(x),\, k \in \mathbb{Z}\} \tag{2.9}$$

where

$$\psi_{j,k}(x) = 2^{j/2}\psi\left(2^j x - k\right) \tag{2.10}$$

and $\psi(x)$ is the wavelet of the multi-resolution analysis which satisfies

$$\psi(x) = 2\sum_k b_k \varphi(2x - k) \qquad x \in \mathbb{R}\,. \tag{2.11}$$

The orthogonality between the space V_j and W_j leads to the relation

$$b_k = (-1)^k \bar{a}_{1-k} \tag{2.12}$$

where 'bar' stands for complex conjugate.

Following (2.7), any function of $L^2(\mathbb{R})$ can be expanded as a linear combinaton of translates of the scaling function $\varphi(x)$ at some fixed scale and the translates of the wavelet $\psi(x)$ expressed at finer scales as

$$f(x) = \sum_k v_{j_0,k}\varphi_{j_0,k}(x) + \sum_{j \geqslant j_0}\sum_k w_{j,k}\psi_{j,k}(x)\,. \tag{2.13}$$

If for some small scale $j_0 = N$ (large N) the second contribution in (2.13) happens to be negligible (it corresponds to the high-frequency component of $f(x)$), then $f(x)$ can be written as the so-called 'wavelet–Galerkin' expansion

$$f(x) \approx \sum_k v_{N,k}\varphi_{N,k}(x)\,. \tag{2.14}$$

Thanks to the orthonormal decomposition (2.8), we then have

$$V_N = V_{N_0} \oplus W_{N_0} \oplus W_{N_0+1} \ldots \oplus W_{N-1} \tag{2.15}$$

for some larger scale $N_0 < N$ (see figure 1). This decomposition amounts to consider the equivalent finite expansion for $f(x)$,

$$f(x) = \sum_k v_{N_0,k}\varphi_{N_0,k}(x) + \sum_{j=N_0}^{N-1}\sum_k w_{j,k}\psi_{j,k}(x)\,. \tag{2.16}$$

In this expansion, the first contribution represents the approximation of $f(x)$ at a given 'coarse' scale. The remaining terms are the corrections at finer scales. Equation (2.16) completely describes the function $f(x)$ within the accuracy of the projection (2.14).

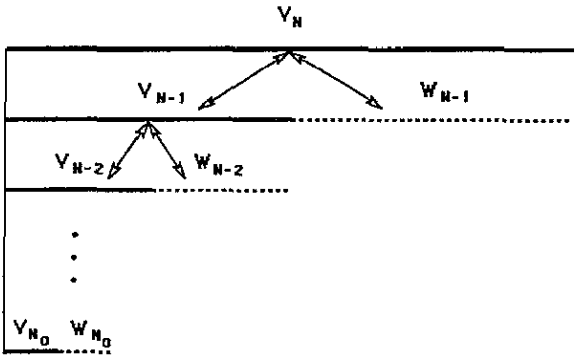

Figure 1. Schematic representation of the multi-resolution analysis. N and N_0 are the finest and coarsest resolution levels, respectively.

2.2. Complex symmetric wavelets

Let us now turn to the construction of the basic ingredient of the multi-resolution analysis: the scaling function $\varphi(x)$. We consider the solutions of (2.1) with four important constraints on $\varphi(x)$:

(i) compactness of its support,
(ii) orthogonality of its translates,
(iii) regularity, and
(iv) symmetry.

The first condition insures an exact local description of the functions of $L^2(\mathbb{R})$. As a consequence, there are a finite number of non-vanishing scaling coefficients a_k and we will consider $a_k \neq 0$ for $k = -J, -J+1, \ldots, J, J+1$, where J is an arbitrary integer. It is straightforward to show that both $\varphi_{j,k}(x)$ and $\psi_{j,k}(x)$ have a support in the interval $[2^{-j}(-J+k), 2^{-j}(J+k+1)]$. The first three conditions define the so-called Daubechies' wavelet analyses [23] for which the regularity condition sets the 'polynomial content' of the V spaces (scaling functions of regularity R ($R \leqslant J$) allow *exact* representations of polynomials of order R in the V spaces). The scaling function and its translations thus define a polynomial interpolation scheme up to order J. In this work, we consider the maximum regularity for a given compact support, i.e. we take $R = J$.

The symmetry requirement has been explored only recently [9]. As already noticed by Lawton [29], the solutions must be complex valued. Figure 2 shows an example of a complex-symmetric scaling function and wavelets for $J = 4$. The values for the a_k's can be found in [9]. When the above four constraints are satisfied, the scaling functions $\varphi_{j,k}(x)$ and the associated wavelet $\psi_{j,k}(x)$ are found to be even and odd, respectively, about the point

$$x_{j,k} = 2^{-j-1} + k2^{-j}. \tag{2.17}$$

The symmetry property of $\varphi(x)$ thus implies that the odd-centred moments vanish, that is,

$$\int \left(x - \tfrac{1}{2}\right)^k \overline{\varphi}(x)\, dx = 0 \qquad k = 1, 3, 5. \tag{2.18}$$

In addition, the second-centred moments ($k = 2$) turn out to be purely imaginary [9]. Property (2.18) helps us to compute the coefficients $v_{N,k}$ of the Galerkin expansion (2.14)

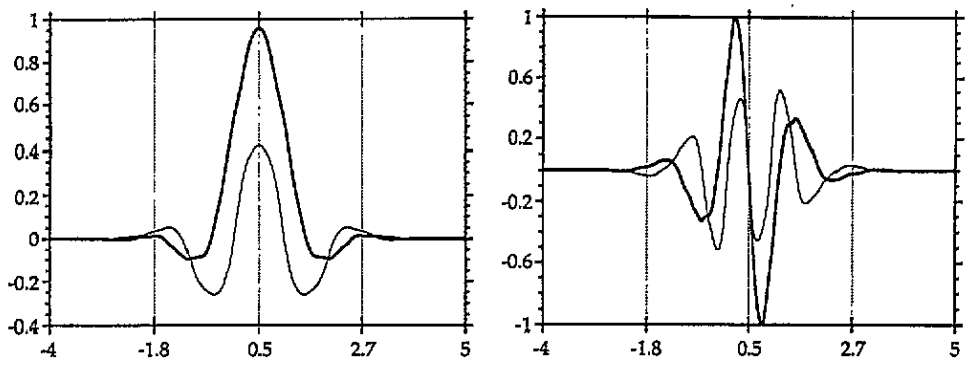

Figure 2. Real part (full curve) and imaginary part of the $J = 4$ complex-symmetric scaling function (upper figure) and wavelet (lower figure).

with good accuracy. In fact, making a Taylor expansion of $f(x)$ around the points $x_{N,k}$ in (2.17) and using the orthogonality and the normalization of the scaling function, the projection of $f(x)$ onto V_N leads to

$$\begin{aligned} v_{N,k} &= \langle \varphi_{N,k} | f \rangle \\ &= 2^{N/2} \int \overline{\varphi}(2^N x - k) f(x)\, \mathrm{d}x \\ &\approx 2^{-N/2} \left[f(x_{N,k}) - \mathrm{i}\gamma 2^{-(2N+1)} \frac{\mathrm{d}^2 f(x_N, k)}{\mathrm{d}x^2} + \cdots \right] \end{aligned} \tag{2.19}$$

where γ is a real coefficient which only depends on J (e.g. $\gamma = 0.322\,748$ for $J = 2$ and $\gamma = 0.178\,936$ for $J = 4$). For sufficiently smooth functions $f(x)$ and large N, the second term in (2.18) can be neglected.

Thanks to (2.1) and (2.11), one can show that the coefficients $v_{j,k}$ and $w_{j,k}$ ($N_0 \leqslant j < N - 1$) can be calculated recursively from $v_{N,k}$ by

$$v_{j-1,k} = \sqrt{2} \sum_m \overline{a}_m v_{j,2k+m} \qquad w_{j-1,k} = \sqrt{2} \sum_m \overline{b}_m v_{j,2k+m}\,. \tag{2.20}$$

Such a transformation will be denoted by $\mathcal{W}$. The orthogonality conditions imply the following inverse for $\mathcal{W}$:

$$v_{j+1,k} = \sqrt{2} \sum_m [a_{k-2m} v_{j,m} + b_{k-2m} w_{j,m}]\,. \tag{2.21}$$

Finally, in the particular application of the present work, the simulation is done for a finite 'spatial window'. This implies that the infinite range of k will be reduced to a finite set by normalizing the spatial sampling of $f(x)$ on the interval $\left[-\frac{1}{2}, \frac{1}{2}\right]$. Since the compact support of the basis functions is finite, the convolutions (2.20) and (2.21) involve a finite number of sampling points outside the window. The field samplings outside the window can, however, be estimated using simple extrapolation techniques; periodization, extrapolation or reflection. We have found it convenient to use periodization when $f(x)$ has finite bandwidth (e.g. bright solitons) and mirror reflection for infinite bandwidth (e.g. dark soliton). The function $f(x)$ will then be written as in (2.16) with only 2^j terms at each level j (see figure 3), corresponding to $-\frac{1}{2} < x_{j,k} < \frac{1}{2}$, i.e.

$$k \in K(j) = \left\{ -2^{j-1}, -2^{j-1} + 1, \ldots, 2^{j-1} - 1 \right\}. \tag{2.22}$$

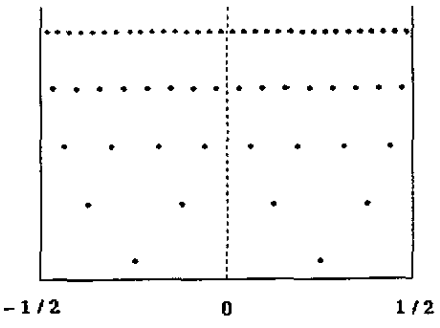

Figure 3. Illustration of the position of the sampling points in the normalized x-window for the simulation. For symmetric wavelets, these points correspond to the centre of the wavelet support.

2.3. *Differential operators*

Let us conclude this section with the description of the differential operator d^n/dx^n in the multi-resolution scheme. Following the expansion (2.15), this amounts to considering the matrix elements of the differential operator in the space V_0, that is

$$c_k^{(n)} = \left\langle \varphi_{0,k}(x) \middle| \frac{d^n\varphi(x)}{dx^n} \right\rangle = \int \bar{\varphi}(x-k)\frac{d^n\varphi(x)}{dx^n}\,dx\,. \tag{2.23}$$

Using (2.1) with an obvious change of variable, we obtain

$$c_k^{(n)} = 2^{n+1} \sum_{m=-2J}^{2J} \sum_{m'=-J}^{J+1} \bar{a}_{m+m'-2k} a_{m'}\, c_m^{(n)}\,. \tag{2.24}$$

The parameters $c_k^{(n)}$ only depend on the wavelet order J and not on the wavelet type for a given J (real, complex symmetric or complex asymmetric).

Equation (2.24) can be cast in the matrix form

$$Ac^{(n)} = \frac{1}{2^{n+1}} c^{(n)} \tag{2.25}$$

where the $(4J+1)\times(4J+1)$ matrix A is the 'Lawton matrix' [26] of components

$$A_{k,k'} = \sum_{m=-J}^{J+1} \bar{a}_{m+k'-2k} a_m\,. \tag{2.26}$$

Therefore the matrix elements of the nth derivative operator in V_0 are the components of an eigenvector of A for the eigenvalue $\lambda_n = 1/2^{n+1}$. Consistency requires that such an eigenvector should be unique for this nth derivative operator to be meaningful. In particular, the $n = 0$ derivative condition is nothing but the orthonormality condition on the translates of $\varphi(x)$. This is the Lawton theorem. The other eigenvalues $\lambda = \frac{1}{4}, \frac{1}{8}, \ldots$ result from the regularity constraints on the scaling coefficients.

Let us mention that for a given n, equation (2.25) only defines the corresponding eigenspace for λ_n. Finding the unique eigenvector $c^{(n)}$ requires an extra relation which normalizes the λ_n-eigenvector. This relation can be derived as follows. Let us define $\Phi_m(x) = \sum_l l^m \varphi(x-l)$. Denoting by $\mathcal{M}_k$ the kth moment of the scaling function, i.e.

$$\mathcal{M}_k = \int \bar{\varphi}(x)x^k dx \qquad \mathcal{M}_0 = 1 \tag{2.27}$$

we can show that

$$\int \bar{\varphi}(x-k)x^n\,\mathrm{d}x = \int \bar{\varphi}(x-k)\Phi_n(x)\,\mathrm{d}x + \sum_{l=1}^{n}\int \binom{n}{l}\mathcal{M}_l\,\bar{\varphi}(x-k)\Phi_{n-l}(x)\,\mathrm{d}x\,. \tag{2.28}$$

Since we consider orthonormal bases and J vanishing moments for the wavelets, i.e.

$$\int \bar{\psi}(x)x^k\,\mathrm{d}x = 0 \qquad 0 \leqslant k \leqslant J \tag{2.29}$$

relation (2.28) yields

$$x^n = \sum_{l=0}^{n}\int \binom{n}{l}\mathcal{M}_l\,\Phi_{n-l}(x)\,. \tag{2.30}$$

By successive derivation of this expression, we obtain

$$\Phi_n^{(n)}(x) = n! \qquad \text{and} \qquad \Phi_n^{(p)}(x) = 0 \quad \forall p > n \tag{2.31}$$

and consequently

$$\sum_{l=-\infty}^{\infty}\int l^n\bar{\varphi}(x)\varphi^{(n)}(x-l) = n!\,. \tag{2.32}$$

Equation (2.32) leads to the normalization condition

$$\sum_{l=-\infty}^{\infty} l^n c_l^{(n)} = (-1)^n n!\,. \tag{2.33}$$

Thus, given an arbitrary eigenvector $r^{(n)}$, the components of $c^{(n)}$ satisfy

$$c_k^{(n)} = \frac{(-1)^n n!}{\sum_{l=-2J}^{2J} l^n r_l^{(n)}}\, r_k^{(n)}\,. \tag{2.34}$$

Notice that this result uniquely defines the nth derivative operator only for $n \leqslant J$. It will be used in the next section to express the NLS equation on the wavelet basis.

3. The basic numerical algorithm

One of the most popular numerical scheme to solve NLS-type equations is the symmetrized split-step Fourier method [21, 27, 28]. This is essentially a pseudo-spectral algorithm which handles the linear and nonlinear parts of the model differently. Because nonlinear terms are more easily calculated in the original spacetime domain, only the linear part is decomposed into its Fourier components.

3.1. The symmetrized split-step method on wavelets

The NLS equation (1.1), and generally any evolution equations of the form

$$u_t = [L + N(t)]u \tag{3.1}$$

where L and $N(t)$ are linear and nonlinear operators, respectively, can be solved formally as

$$u(t_2) = e^{\mathcal{L}+\mathcal{N}}\, u(t_1) \tag{3.2}$$

where $\mathcal{L} = (t_2 - t_1)\, L$, $\mathcal{N} = \int_{t_1}^{t_2} N(t)\, dt$ and t_1, t_2 are the initial and final times, respectively.

In general, linear and nonlinear effects act together during the evolution and cannot be handled separately. Mathematically, this results from the fact that $\mathcal{L}$ and $\mathcal{N}$ do not commute, that is, $e^{\mathcal{L}+\mathcal{N}} \neq e^{\mathcal{L}} e^{\mathcal{N}}$. The essence of the split-step method consists in assuming that for a small time-step $\Delta t = t_2 - t_1$, we can pretend that the linear and nonlinear terms act independently such that

$$u(t_2) \cong e^{\mathcal{L}/2} e^{\mathcal{N}} e^{\mathcal{L}/2} u(t_1)\,. \tag{3.3}$$

Relation (3.3) is the basic scheme of the numerical algorithm.

The main interest in the method is that the execution of the linear operator $e^{\mathcal{L}/2}$, when carried out in the Fourier domain, can be calculated numerically very quickly. The Fourier basis is, however, not well adapted to high gradient phenomena since the basis elements are globally defined. In contrast, the wavelet basis is a local one and the linear evolution can, of course, be calculated on it. In particular, one can project the field on a space V_N, where 2^N is the number of field samples (the wavelet–Galerkin method), or make a wavelet transformation of it, that is, decompose the field on $\ldots W_{N-3} \oplus W_{N-2} \oplus W_{N-1}$. In both cases the projection can easily be implemented using the same numerical algorithm without discarding the essential features of the time-step splitting. Schematically, the evolution over one time-step Δt follows the symmetrized split-step method except that the Fourier transform $\mathcal{F}$ is replaced by a projection $\mathcal{P}_N$ onto V_N or by a wavelet transform $\mathcal{W}$ on $V_{N_0} \oplus W_{N_0} \oplus W_{N_0+1} \ldots \oplus W_{N-1}$, together with the appropriate representation of the second derivative operator. Finally, the nonlinearity can be treated in the finest resolution space V_N.

3.2. The wavelet–Galerkin projection

For now, let us concentrate on the wavelet–Galerkin procedure. We will go back to the wavelet projection in section 5. Suppose the field $u(t, x)$ has been regularly sampled over 2^N points on the interval $\left[-\frac{1}{2}, \frac{1}{2}\right]$. Projecting $u(t, x)$ onto V_N, we obtain

$$u(t, x) = \sum_{k=-2^{N-1}}^{2^{N-1}-1} 2^{-N/2} u_{N,k}(t) \varphi_{N,k}(x) \tag{3.4}$$

where $u_{N,k}(t) = u(t, x_{N,k})$ and $x_{N,k} = \frac{1+2k}{2^{N+1}}$ are the collocation (sampling) points. The advantage of knowing the field projection on V_N is that one can easily calculate the nonlinear term using a simple collocation procedure. In fact, if the sampling is dense enough, the nonlinear term $|u(t, x)|^{2\sigma}$ can be estimated from (3.4) with coefficients $2^{-N/2}|u_{N,k}(t)|^{2\sigma}$. This will be used throughout all our simulations to calculate the nonlinear effects.

The main difference between Fourier and wavelet scaling functions bases lies in the representation of the second space derivative [30, 31]. In particular, this operator is no longer diagonal in the scaling function basis.

Substituting (3.4) into $iu_t + \frac{1}{2}u_{xx} = 0$, multiplying from the left by $\bar{\varphi}_{N,l}(x)$, integrating over $-\infty < x < \infty$ and making use of the orthogonality relations between translated scaling functions, leads to an equation of the form

$$\frac{\mathrm{d}}{\mathrm{d}t}u_N = \tfrac{1}{2}\mathrm{i}T_N u_N \tag{3.5a}$$

where

$$(T_N)_{kl} = \int \bar{\varphi}_{N,k}\frac{\mathrm{d}^2}{\mathrm{d}x^2}\varphi_{N,l}\,\mathrm{d}x = 2^{2N+3}\sum_{m=-J}^{J+1}\sum_{m'=-J}^{J+1}\bar{a}_m a_{m'}c^{(2)}_{2(k-l)+m-m'}\,. \tag{3.5b}$$

The matrix T_j is a band-diagonal matrix having the same $4J + 1$ non-vanishing elements on each row. Equation (3.5) can be solved exactly as

$$u_N(t_2) = \mathrm{e}^{\mathrm{i}(t_2-t_1)T_N/2}u_N(t_1)\,. \tag{3.6}$$

As mentioned in section 2, the coefficients $c_l^{(2)}$ only depend on the wavelet order J and not on the wavelet-type. This is not the case for the matrix T_N. In particular, T_N turns out to be real and symmetric for complex-symmetric scaling functions.

The value of the coefficients $c_l^{(2)}$ for the wavelet used in this work, i.e. $J = 2$, 4 and 8, are given in table 1.

Table 1. Values of the coefficients $c_l^{(2)}$ for the second derivative operator.

$c_l^{(2)}$ $(= c_{-l}^{(2)})$	$J = 2$	$J = 4$	$J = 8$
$c_0^{(2)}$	$-\frac{885}{168}$	−3.834 994 313 783 547 318	−3.518 861 054 010 038
$c_1^{(2)}$	$\frac{356}{105}$	2.414 790 351 192 872 32	2.194 072 686 579 494 1
$c_2^{(2)}$	$-\frac{92}{105}$	−0.649 502 189 980 784 786 2	−0.610 929 112 091 214 9
$c_3^{(2)}$	$\frac{12}{105}$	0.180 953 550 093 409 320 1	0.247 332 322 694 628 9
$c_4^{(2)}$	$\frac{3}{560}$	−0.029 907 980 437 657 401 96	−0.094 970 844 750 517 18
$c_5^{(2)}$		0.000 794 620 557 143 6	0.030 068 613 612 554 4
$c_6^{(2)}$		0.000 367 145 383 89	−0.007 248 478 692 850 98
$c_7^{(2)}$		0.000 001 656 544 136 04	0.001 230 499 099 443 004
$c_8^{(2)}$		0.000 000 003 538 760 056	−0.000 133 610 006 425 686
$c_9^{(2)}$			0.000 009 130 930 738 6
$c_{10}^{(2)}$			−0.000 000 734 346 69
$c_{11}^{(2)}$			0.000 000 047 555 795 9
$c_{12}^{(2)}$			0.000 000 006 327 051 767
$c_{13}^{(2)}$			0.000 000 000 049 283 6
$c_{14}^{(2)}$			0.000 000 000 000 279 3
$c_{15}^{(2)}$			$2.953\,25 \times 10^{-16}$
$c_{16}^{(2)}$			1.7699×10^{21}

3.3. Accuracy considerations between Fourier and wavelet–Galerkin projections

It is instructive to compare the accuracy of the split-step Fourier and wavelet–Galerkin numerical schemes. Only typical results, using the fundamental soliton solution of the cubic NLS'+' equation as a benchmark, will be presented here. For $\lambda = 1$, this exact solution is

$$u(t, x)_{\text{sol}} = \operatorname{sech}(x - vt)\, e^{ivx + i(1-v^2)t/2} \tag{3.7}$$

where v is the soliton speed. The parameter v has not been normalized to 0 using the Galilean boost symmetry of (1.1) since this symmetry is broken by the spacetime numerical discretization. The other two free parameters, the amplitude and phase, have been normalized to 1 and 0, respectively, using the dilatation and constant phase symmetries of (1.1).

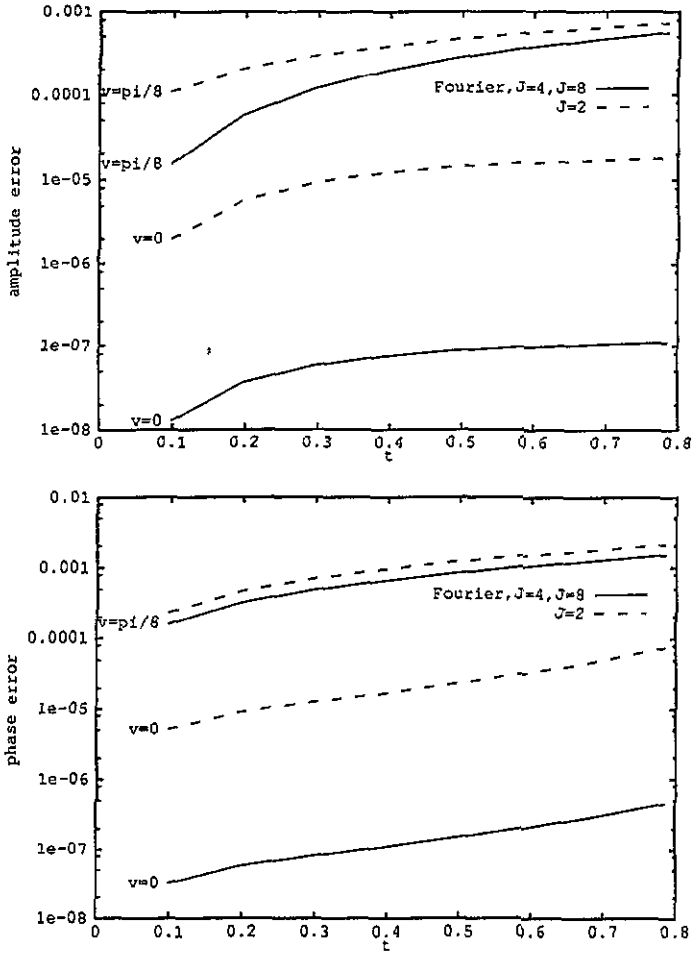

Figure 4. Evolution of the mean square error on the field amplitude and phase for the stationary ($v = 0$) and moving ($v = \pi/8$) fundamental soliton solution using Fourier and wavelet–Galerkin projections with $J = 2$, 4 and 8.

We have compared solution (3.6) to its numerical simulation (with initial condition $u(0,x)_{\text{sol}}$) for $v = 0$ and $v = 8/\pi$ using Fourier and $J = 2$, 4 and 8 scaling function bases, over a time range of $\pi/4$ with 1024 sampling points and a time-step of $\Delta t = \pi/2560$. The mean square error on the amplitude and phase is calculated over the 256 central samples using the formula

$$\text{error} = \left[\Delta x \sum_{i} |F_i^{\text{exact}} - F_i^{\text{num}}|^2\right]^{1/2} \tag{3.8}$$

where Δx is the space-step and F is the amplitude or phase. The results are depicted in figure 4, which gives the evolution of the errors at a regular time interval of $\pi/32$. The $J = 2$ basis is always less accurate than Fourier, $J = 4$ and 8; up to 100 times less accurate for $v = 0$. This can be explained by the fact that, even though the second derivative operator can be represented on the $J = 2$ wavelet basis, the scaling function and wavelet *are not* $C^{(2)}$. The cases $J = 4$ (which is almost $C^{(2)}$) and $J = 8$ give the same error as Fourier for the test function (3.7). Note that more irregular test functions could lead to different results for $J = 4$ and 8 if their representation in terms of fourth-order polynomials is not accurate enough.

In view of the above results, for the rest of the work we choose a multi-resolution space of order $J = 4$ for our simulations. The $J = 8$ basis will only be used in the up-sampling scheme which will be described in the following section. We believe that this possibility of mixing wavelet orders, i.e. regularity levels, in a numerical scheme is an advantage over standard numerical methods and should be exploited in other applications of wavelets.

4. A globally adaptive algorithm

4.1. Description

This section concerns a global adaptive grid for the split-step Fourier or wavelet–Galerkin methods described in section 3. More precisely, we want to show how regularity properties of scaling functions can be used to increase (or decrease) the field sampling over the entire x-window during the simulation [32]. In particular, for the Fourier projection, this results in an efficient hybrid numerical algorithm which combines the rapidity of the split-step method for calculating the time evolution and the interpolation properties of scaling functions for the up-sampling process.

[t]

The idea is the following. At the beginning of each time-step, one performs a one-level wavelet transform of the field $u(t,x)$ from the sampling level j to level $j-1$, in order to detect the presence of strong gradients. When the maximal absolute value of the wavelet coefficients w_{j-1} is greater that a predetermined threshold (fixed to 0.005 in our simulations), the number of collocation points is doubled using an interpolation process on the field sampling at level j. This should be done by performing a transform $\mathcal{T}$, from level j to level $j+1$, of the 2^j field samples v_j with the 2^j wavelet coefficients w_j set to zero. The result of this transformation should be a set of 2^{j+1} scaling coefficients v_{j+1} which constitute the new field sampling (after multiplying by a $\sqrt{2}$ normalization factor). An important point to be careful about is that no local asymmetry is introduced during the up-sampling process. This is where the symmetry properties of the complex scaling functions are useful. Unfortunately, a recomposition

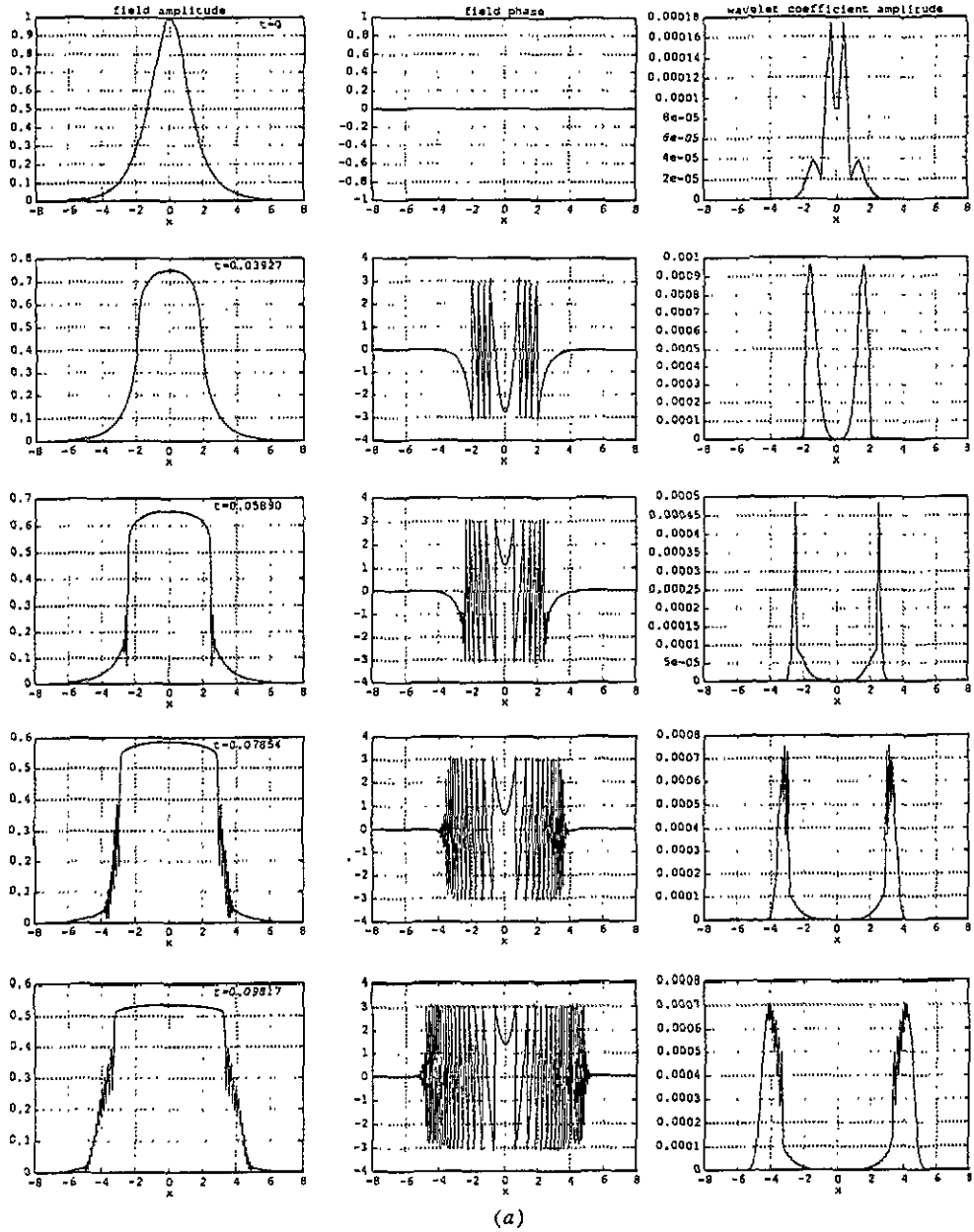

Figure 5. *(a) Evolution of the field amplitude, field phase and wavelet coefficient amplitude* for typical breaking-wave phenomena in the cubic NLS'−' equation and *(b)* variation of the maximum amplitude wavelet coefficient during the adaptive simulation.

using complex scaling functions slightly couples the real and imaginary parts of the field $u(t, x)$ (for instance, by introducing imaginary components in v_{j+1} on an initial real field v_j). This can be avoided, by up-sampling the field, using a linear combination of the inverse wavelet transform and its complex conjugate, that is $\mathcal{T} = \frac{1}{2}(\mathcal{W}^{-1} + \overline{\mathcal{W}}^{-1})$; in order words, by up-sampling the field using the real part of the coefficients a_k only.

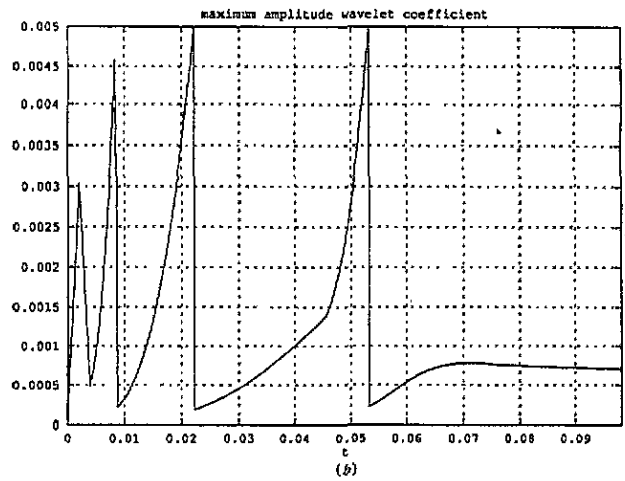

Figure 5. (Continued)

In fact, we have found this recomposition scheme very accurate, provided that the order of the up-sampling scaling function is larger than the order of the decomposition wavelet. The reason is that the second centred moment of the scaling function $\varphi(x)$, that is $\int \left(x-\frac{1}{2}\right)^2 \bar{\varphi}(x)\,dx$, is purely imaginary and decreases with order J. In addition, $\int \left(x-\frac{1}{2}\right)^k \bar{\varphi}(x)\,dx = 0$ for odd values of k since $\varphi(x)$ is symmetric. In our simulations, we have chosen to up-sample with the $J = 8$ scaling function and decompose with the $J = 4$ wavelet.

4.2. Applications

We have written a C program which performs the above-described global recomposition. Both Fourier and wavelet pseudo-spectral methods described in section 3 have been tested and have given similar results. Fast Fourier transforms and complex structures have been implemented using standard techniques [33]. A decrease in the time-step by a factor of 4 is done after each up-sampling in order to keep numerical stability. The maximum wavelet amplitude for the up-sampling threshold has been fixed to 0.005.

Figure 5 shows a first simulation leading to high-field gradients. This is a typical 'breaking-wave' phenomena in optics which appears in the normal dispersion regime, that is, for the cubic NLS'$-$' equation with $\lambda < 0$. In this simulation, $\lambda = -900$, the initial field $u(0,x) = \mathrm{sech}(x)$ has been sampled 128 times, the time range is $\pi/32$ and the initial time-step has been set to $\pi/1600$. The amplitude of the wavelet coefficients $w(t)$ is quite instructive of the sharp field structure evolution. Figure 5(b) shows the evolution of the maximal amplitude of the wavelet coefficients as t increases. Each peak is the result of a new sampling. The final number of collocation points is 2048. A comparison with a non-adaptive simulation (with 2048 samples and the corresponding $\Delta t = \pi/409\,600$) shows that the accuracy of the adaptive simulation is quite satisfactory. In fact, no difference can be detected on the amplitude and phase from the plots. Only the wavelet coefficients w_{j-1}, where j is the sampling level, are sufficiently sensitive to show that the slight ripples around $|x| = 2$ at the end of the simulation are absent in the non-adaptive simulation (see the bottom right-hand plot on figure 5(a)).

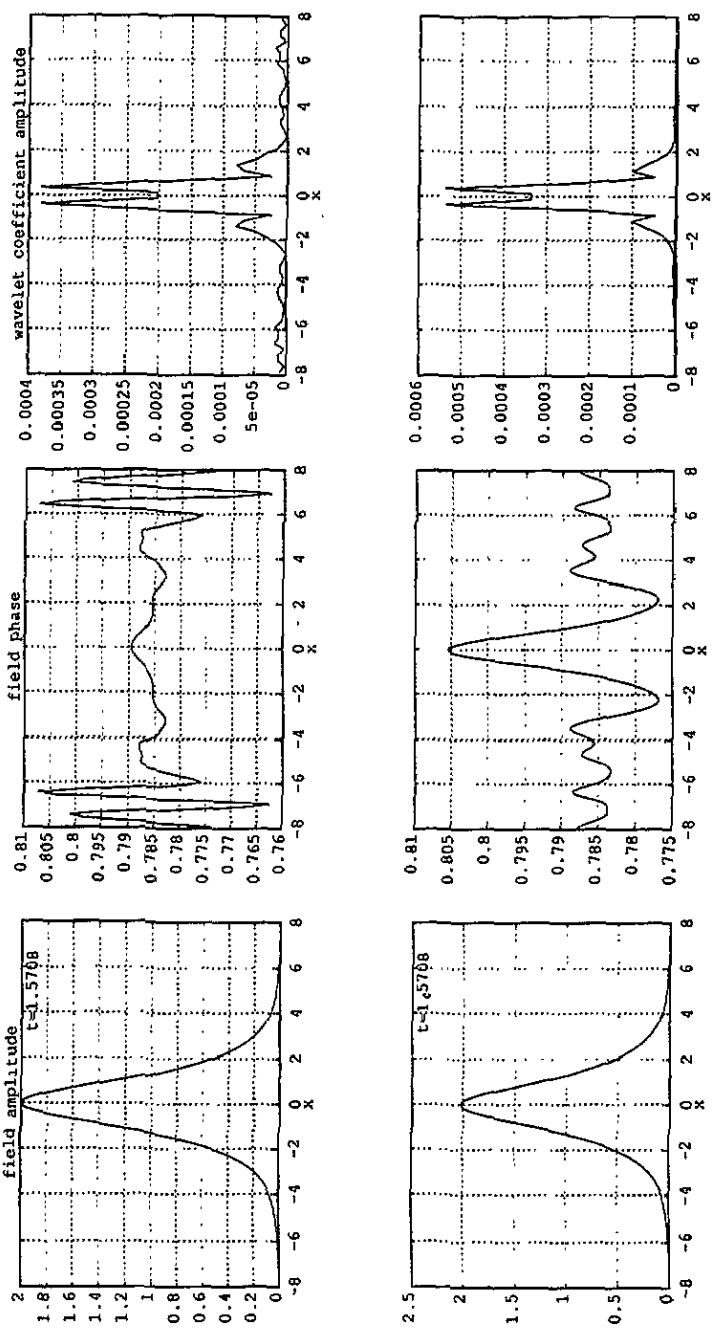

Figure 6. (*a*) Evolution of the field amplitude, field phase and wavelet coefficient amplitude for a typical collapse phenomena in the quintic NLS '+' equation and (*b*) variation of the maximum amplitude wavelet coefficient during the adaptive simulation.

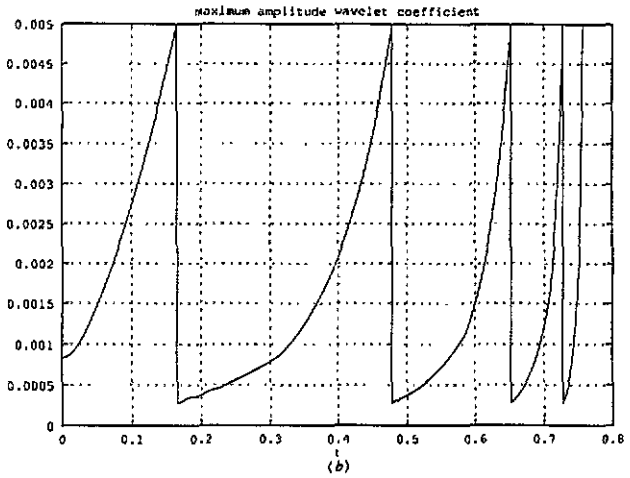

Figure 6. (Continued)

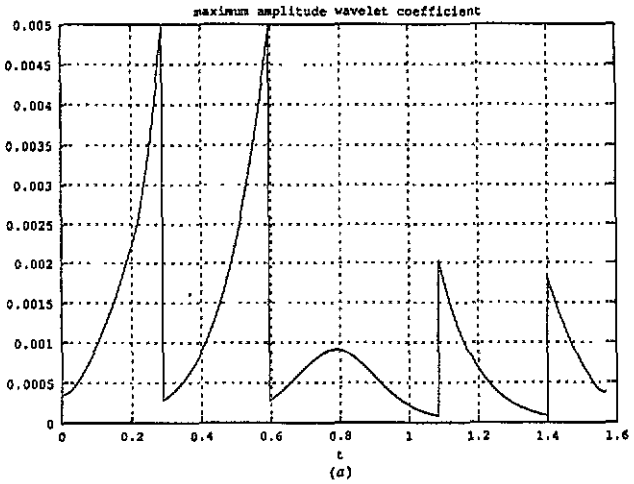

Figure 7. (*a*) Variation of the maximum amplitude wavelet coefficient during the adaptive simulation of the two-soliton solution of the cubic NLS'+' equation and (*b*) field amplitude, field phase and wavelet coefficient amplitude after one period with and without adaptivity (first and second row, respectively).

A second simulation generating high gradients is shown on figure 6. This is a typical 'blow-up' phenomena which can be observed for the NLS'+' equation whenever the space dimension D and the nonlinear coefficient σ are related through $\sigma D \geqslant 2$ [19–21]. In this case, any initial condition having a L^2-norm larger than the critical value fixed by the L^2-norm of the fundamental solitary wave solution evolves toward a singularity. In our case ($D = 1$ and $\sigma = 2$) the exact expression for the solitary wave can be normalized to

$$u_{\mathrm{sol}}(t, x) = \tfrac{3}{8}^{1/4} \mathrm{sech}^{1/2}(x)\, \mathrm{e}^{\mathrm{i}t/8}. \tag{4.1}$$

The initial condition in figure 6(*a*) has been chosen as $1.5u_{\mathrm{sol}}(0, x)$ with only 64 samples and $\Delta t = 0.97\pi/320$. The maximum sampling has been fixed at 2048 points. As shown

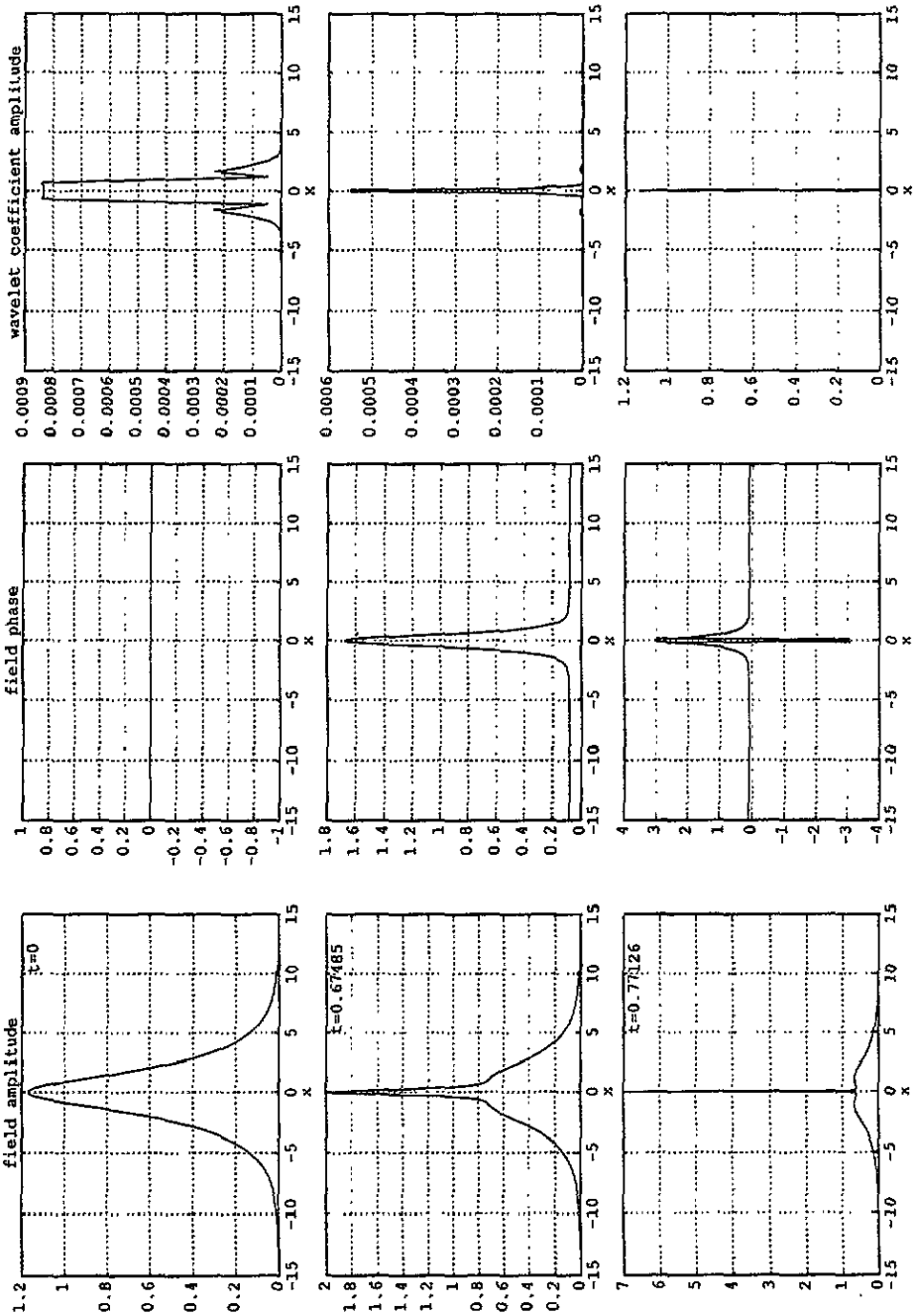

(*b*)

Figure 7. Continued.

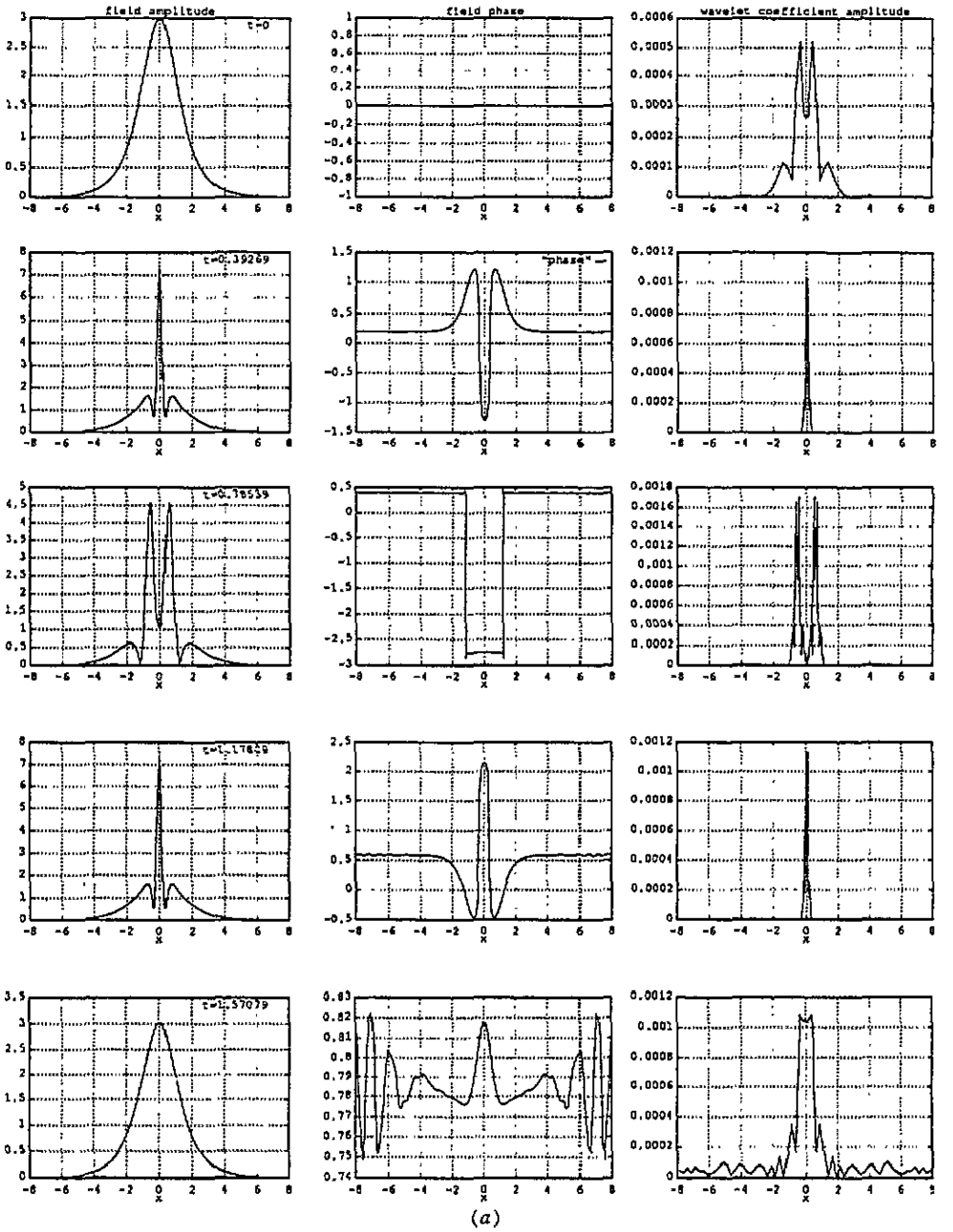

Figure 8. (*a*) Evolution of the field amplitude, field phase and wavelet coefficient amplitude for the bound three-soliton solution of the cubic NLS '+' equation and (*b*) variation of the maximum amplitude wavelet coefficient during the adaptive simulation.

on figure 6(*b*), the field evolves through five successive up-samplings up to 2048 points. At the end of the simulation, a very sharp peak is generated (over a large pedestal). Our up-sampling process has been able to handle such a high gradient effect.

The above adaptive algorithm can also be modified to allow a decrease in the number

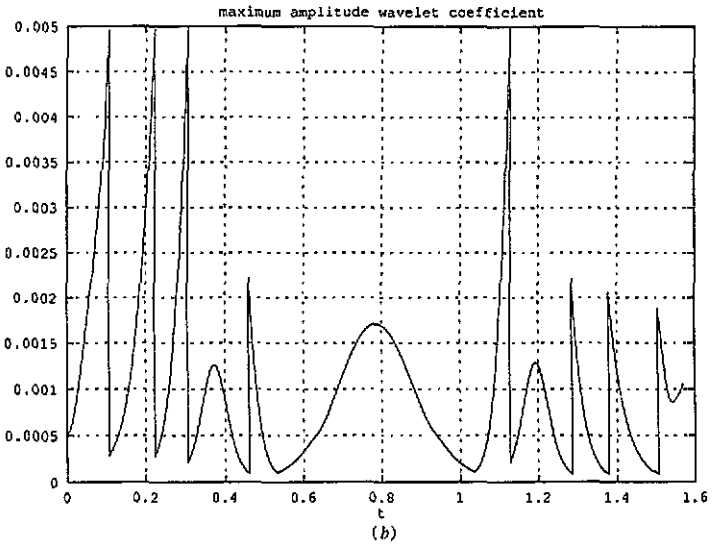

Figure 8. (Continued)

of sampling points when sharp gradients tend to vanish. Similarly to above, the new field sampling $u(t, x_{x_{N-1},k}) = 2^{(N-1)/2} v_{N-1}$ can be obtained form the scaling coefficients v_N using the inverse $\mathcal{T}^{-1}$ of the above up-sampling transform $\mathcal{T}$.

Interesting solutions which can be used to test this idea are the breather (or bounded soliton) solutions of the cubic NLS'+' equation. These are solutions where the amplitude evolves periodically in time, with a period of $\pi/2$, through successive amplitude peakings. They correspond to the initial conditions

$$u(0, x)_{\text{bre}} = N\text{sech}(x) \tag{4.2}$$

where N is the solution order (the number of solitons involved in the solution).

Figure 7(a) shows the variation of the maximal amplitude of the wavelet coefficients with adaptivity for the case $N = 2$, over one period ($t = \pi/2$) with 128 initial samples and $\Delta t = \pi/2560$. The upper threshold has been fixed to 0.005 and the lower one to 30% of the maximal wavelet amplitude obtained after the first up-sampling. This is to avoid a premature decreasing of the sampling due to the oscillatory structures (see figure 7(a)) during the up-sampling relaxation time. The sample number goes up to 512 at the half-period where a peak structure arises in the field amplitude.

Although the up-sampling process is very accurate for the field amplitude, the field phase is more sensitive to it. This is illustrated, for instance, in figure 7(b), which compares the field amplitude, phase and wavelet amplitude coefficients at the end of the simulation obtained for the above adaptive grid (first row) and a fixed 128 points simulation with $\Delta t = \pi/2560$ (second row). One observes that the field amplitude is more accurate for the adaptive simulation. The same observation stands for the central region of the phase. However, the phase has a more important oscillatory structure at the window limits than the non-adaptive scheme (5% of the theoretical value of $\pi/4$ rather than 0.2% for the non-adaptive algorithm). One can improve the accuracy by increasing the initial sampling rate and/or decreasing the up-sampling level. In any case, this cannot be considered as a major drawback of the algorithm since the field amplitude is very small at the window.

Finally, figure 8 shows the numerical simulation for the $N = 3$ breather using the same initial parameters as the $N = 2$ case. The number of collocation points varies as 128–256–512–1024–512–1024–512–256–128, following the periodicity in the field evolution. One observes that the periodicity of the field amplitude is well described. Taking into account that four up-samplings and four sub-samplings have been performed during the simulation, the 10% accuracy on the phase, with respect to the theoretical value of $\pi/4$, is very satisfactory.

5. A locally adaptive algorithm

In the previous section, we have used wavelets (or more precisely scaling functions) as an interpolating tool for implementing a global adaptive grid. We will now concentrate on local adaptivity using the multi-resolution property of the wavelet basis. In this paper, we will restrict ourselves to the description of the numerical algorithm. Its implementation and testing will be reported later.

5.1. Linear evolution on wavelet bases

Let us first recap on how the linear part of the NLS equation is projected onto the wavelet basis. The first step is to calculate the matrix representation of the second-derivative operator in the wavelet basis. Suppose the field $u(t, x)$ has been sampled 2^N times and projected onto V_N as in (3.1). Using the multi-resolution decomposition of V_N up to a coarsest resolution 2^{N_0}, $N_0 \leqslant N$, one obtains

$$u(t,x) = \sum_{k=-2^{N_0-1}}^{2^{N_0-1}-1} v_{N_0,k}(t)\varphi_{N_0,k}(x) + \sum_{j=N_0}^{N-1}\sum_{k=-2^{j-1}}^{2^{j-1}-1} w_{j,k}(t)\psi_{j,k}(x)\,. \tag{5.1}$$

The corresponding scaling and wavelet coefficients contains the 'averaged' and 'detailed' information on $u(t, x)$ at a given time t, in the transformed space. Substituting (5.1) into $iu_t + \frac{1}{2}u_{xx} = 0$, multiplying from the left by $\bar{\varphi}_{N_0,l}(x)$ and $\bar{\psi}_{i,l}(x)$, integrating over $-\infty < x < \infty$ and making use of the orthogonality relations between scaling and wavelet functions, leads to an equation of the form

$$\frac{\mathrm{d}}{\mathrm{d}t}\begin{pmatrix} w_{N-1} \\ \vdots \\ w_{N_0+2} \\ w_{N_0+1} \\ w_{N_0} \\ v_{N_0} \end{pmatrix} = \tfrac{1}{2}\mathrm{i}M \begin{pmatrix} w_{N-1} \\ \vdots \\ w_{N_0+2} \\ w_{N_0+1} \\ w_{N_0} \\ v_{N_0} \end{pmatrix} \tag{5.2a}$$

where

$$M = \begin{pmatrix} A_{N-1} & \cdots & A^{N-1}_{N_0+2} & A^{N-1}_{N_0+1} & A^{N-1}_{N_0} & B^{N-1}_{N_0} \\ \vdots & \ddots & \vdots & \vdots & \vdots & \vdots \\ A^{N_0+2}_{N-1} & \cdots & A_{N_0+2} & A^{N_0+2}_{N_0+1} & A^{N_0+2}_{N_0} & B^{N_0+2}_{N_0} \\ A^{N_0+1}_{N-1} & \cdots & A^{N_0+1}_{N_0+2} & A_{N_0+1} & A^{N_0+1}_{N_0} & B^{N_0+1}_{N_0} \\ A^{N_0}_{N-1} & \cdots & A^{N_0}_{N_0+2} & A^{N_0}_{N_0+1} & A_{N_0} & B_{N_0} \\ \Gamma^{N_0}_{N-1} & \cdots & \Gamma^{N_0}_{N_0+2} & \Gamma^{N_0}_{N_0+1} & \Gamma_{N_0} & T_{N_0} \end{pmatrix} \tag{5.2b}$$

and A, B, Γ and T are band matrices whose elements are

$$(A_j^{j'})_{kl} = \int \tilde{\psi}_{j',k} \frac{d^2}{dx^2} \psi_{j,l}\, dx \qquad A_j^J \equiv A_j \tag{5.3a}$$

$$(B_j^{j'})_{kl} = \int \tilde{\psi}_{j',k} \frac{d^2}{dx^2} \varphi_{j,l}\, dx \qquad B_j^j \equiv B_j \tag{5.3b}$$

$$(\Gamma_j^{j'})_{kl} = \int \bar{\varphi}_{j',k} \frac{d^2}{dx^2} \psi_{j,l}\, dx \qquad \Gamma_j^j \equiv \Gamma_j \tag{5.3c}$$

$$(T_j)_{kl} = \int \bar{\varphi}_{j,k} \frac{d^2}{dx^2} \varphi_{j,l}\, dx\,. \tag{5.3d}$$

Matrices A_j, B_j, Γ_j and T_j have $4J+1$ non-vanishing elements on each row. Matrices A_j and T_j are real and symmetric while $\Gamma_j = (B_j)^\dagger$. For complex-symmetric wavelets, the complete matrix M is Hermitian. For real wavelets, it is symmetric.

Equation (5.2) can be solved exactly as

$$\begin{pmatrix} w_{N-1}(t_2) \\ \vdots \\ w_{N_0+2}(t_2) \\ w_{N_0+1}(t_2) \\ w_{N_0}(t_2) \\ v_{N_0}(t_2) \end{pmatrix} = e^{i(t_2-t_1)M/2} \begin{pmatrix} w_{N-1}(t_1) \\ \vdots \\ w_{N_0+2}(t_1) \\ w_{N_0+1}(t_1) \\ w_{N_0}(t_1) \\ v_{N_0}(t_1) \end{pmatrix}. \tag{5.4}$$

The matrix elements for M can be calculated once and for all and stored in memory. To facilitate this calculation, we can use the fact that operators $A_j^{j'}$, with $j < j'$, can be obtained by applying a wavelet transform to each row of all operators B_j. Similarly, operators $A_j^{j'}$, with $j' < j$, can be calculated by applying a wavelet transform on each column of operators Γ_j. These matrices A_j, B_j, Γ_j and T_j can be expressed in terms of the coefficients c_l of section 2 as

$$(A_j)_{kl} = 2^{2j+3} \sum_{m=-J}^{J+1} \sum_{m'=-J}^{J+1} \bar{b}_m b_{m'} c^{(2)}_{2(k-l)+m-m'} \tag{5.5a}$$

$$(B_j)_{kl} = 2^{2j+3} \sum_{m=-J}^{J+1} \sum_{m'=-J}^{J+1} \bar{b}_m a_{m'} c^{(2)}_{2(k-l)+m-m'} \tag{5.5b}$$

$$(\Gamma_j)_{kl} = 2^{2j+3} \sum_{m=-J}^{J+1} \sum_{m'=-J}^{J+1} \bar{a}_m b_{m'} c^{(2)}_{2(k-l)+m-m'} \tag{5.5c}$$

$$(T_j)_{kl} = 2^{2j+3} \sum_{m=-J}^{J+1} \sum_{m'=-J}^{J+1} \bar{a}_m a_{m'} c^{(2)}_{2(k-l)+m-m'} \tag{5.5d}$$

where $c_l^{(2)}$ are given in table 1.

Finally, a second and more practical way to calculate the matrix M is to perform a two-dimensional wavelet transformation of the matrix T_N. For tensor product wavelet bases, this consists of performing a one-dimensional wavelet transform on the rows of T_N followed by the *complex conjugate of the one-dimensional wavelet transform* on the columns. When using complex-symmetric wavelets, the complex conjugacy is necessary in order to conserve the covariance property of the differential operator. An example of the band structure for matrices A_5, A_4^5, A_3^5 and B_3^5 (i.e. $N_0 = 3$) is given in figure 9 for $J = 2$. Full circles give the position of the non-vanishing elements. Open circles represent elements that must be added to periodize the operator.

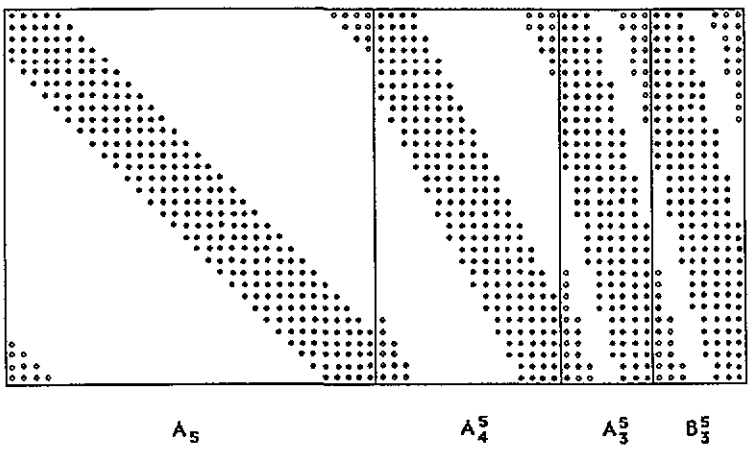

Figure 9. Example of non-vanishing matrix elements in wavelet basis $J = 2$ for the second-derivative operator. Open circles represent elements that periodize the operator.

5.2. Numerical algorithm

The proposed pseudo-spectral algorithm can be summarized in the following pseudo-code. It involves a local wavelet adaptive grid [4, 5, 7, 8] as well as a global up-sampling. For simplicity, we will restrict the description to an algorithm which can only *increase* the resolution.

At the beginning of a time-step ($t = t_1$), the field is supposed to belong to V_j ($j \geqslant N_0$). The field samplings are known, i.e. the scaling coefficients $v_j(t_1)$.

1. Makes a wavelet decomposition up to the coarsest scale 2^{N_0}, that is decompose on $V_{N_0} \oplus W_{N_0} \oplus W_{N_0+1} \oplus \cdots \oplus W_{j-1}$.

- Keeps only the coefficients $w_i(t_1)$ ($i \geqslant N_0$) that are larger than a resolution threshold S_1 (for instance, $S_1 = 0.0005$).
- Checks if $\max(|w_{j-1}(t_1)|)$ is larger than a up-sampling threshold S_2 (for instance, $S_2 = 0.005$).

If YES:

- Adds coefficients $w_j(t_1) = 0$ to the $v_j(t_1)$ ones, up-samples the field on V_{j+1} and stores in memory.
- Decomposes the field on $V_{N_0} \oplus W_{N_0} \oplus W_{N_0+1} \oplus \ldots \oplus W_j$.
- Keeps only the coefficients $w_i(t_1)$ for which $|w_i(t_1)| > S_1$.
- $j = j + 1$
- GOTO 2

If NO:

2. Calculates the linear evolution on the first $\Delta t/2$ interval.

- Recomposes the field on V_j.
- Calculates the nonlinear effects on the field samplings $v_j(t_1 + \Delta/2)$ using the $v_j(t_1)$.
- Decomposes the field into its wavelet coefficients up to V_{N_0}.
- Keeps only the wavelet coefficients for which $|w_i(t_1)| > S_1$.
- Calculates the linear evolution on the second $\Delta t/2$ interval.
- Keeps only the wavelet coefficients for which $|w_i(t_1)| > S_1$.
- Recomposes the field on V_j and stores in memory.
- GOTO 1.

Notice that the above algorithm is a modification of the wavelet-based adaptive numerical method developed in [4, 8]. The main differences are: (i) the pseudo-spectral nature, i.e. linear evolution calculated on $V_{N_0} \oplus W_{N_0} \oplus W_{N_0+1} \oplus \cdots \oplus W_{N-1}$ and nonlinearity on V_N, and (ii) the inclusion of a global up-sampling from V_N to V_{N+1} using the method described in section 4. The pseudo-spectral characteristic is always an important advantage in reducing the complexity of the numerical calculation when higher-order nonlinear effects are added to the original model as, for instance, in the modelling of very short pulses in nonlinear optical fibres [14, 34, 35]. In addition, the global adaptive part does not limit the maximal sampling rate to the sampling rate of the initial field.

6. Conclusion

Wavelets have various fields of application which go well beyond signal analysis [36]. Numerical simulation on wavelet bases is one of them. Here, we have proposed and studied a simple way to dynamically change the sampling rate of a signal which evolves through high-gradient phenomena. The method was based on the interpolation properties of highly regular complex-symmetric scaling functions. We have tested our scheme on the physically relevant cubic and quintic nonlinear Schrödinger equations, for three typical high-gradient solutions: optical breaking wave, collapse and bound solitons. In all these cases, the up-sampling process turned out to be stable and quite accurate.

We have also proposed a modification of the wavelet-based local adaptive numerical method studied in [4, 8] which conserves the pseudo-spectral nature of the split-step method, i.e. linear evolution calculated on $V_{N_0} \oplus W_{N_0} \oplus W_{N_0+1} \oplus \cdots \oplus W_{N-1}$ and nonlinearity on V_N. We think this should be an important advantage in reducing the complexity of the numerical algorithm implementation when higher-order nonlinear effects are added to the original model. In addition, the global adaptive method described in this paper can also be used in conjunction with the local one, when a field up-sampling from V_N to V_{N+1} is necessary. Actual investigations concern the implementation of this scheme and its test on other typical high-gradient simulations such as edge diffraction, step-index medium and two-dimensional self-focusing.

References

[1] Liandrat J, Perrier V and Tchamitchian P 1989 Numerical resolution of the regularized Burgers equation using the wavelet transform *Technical Report* CPT-89/P.2320 Center of Theoretical Physics, Marseille

[2] Glowinski R, Lawton W M, Ravachol M and Tenenbaum E 1989 Wavelet solution of linear and nonlinear elliptic, parabolic and hyperbolic problems in one space dimension *AWARE Technical Report* AD890527.1

[3] Latto A and Tenenbaum E 1990 Compactly supported wavelets and the numerical solution of Burgers' equation *C. R. Acad. Sci., Paris I* **311** 903

[4] Liandrat J and Tchamitchian P 1990 Resolution of the 1D regularized Burgers equation using a spatial wavelet approximation *NASA Report, ICASE Report* no 90-83

[5] Maday Y, Perrier V and Ravel J C 1991 Adaptivité dynamique sur bases d'ondelettes pour l'approximation d'équations aux dérivées partielles *C. R. Acad. Sci., Paris I* **312** 405

[6] Qian S and Weiss J 1992 Wavelets and the numerical solutions of partial differential equations *AWARE Technical Report* AD920318

[7] Jaffard S 1992 Wavelet methods for fast resolution of elliptic problems *SIAM. J. Numer. Anal.* **29** 965

[8] Bacry E, Mallat S and Papanicolaou G 1992 A wavelet spacetime adaptive numerical method for partial differential equations *Math. Mod. Num. Anal.* **26** 793

[9] Lina J M and Mayrand M 1993 Complex Daubechies wavelets *Preprint* Univ. de Montréal *Appl. Comp. Harm. Anal.* submitted

[10] Lina J M and Mayrand M 1994 Parametrization for Daubechies wavelets *Phys. Rev.* E **48** 4160
[11] Ablowitz M J and Segur H 1981 *Solitons and the Inverse Scattering Transform* (Philadelphia, PA: SIAM)
[12] Dodd R K, Eilbeck J C, Gibbon J D and Morris H C 1982 *Solitons and Nonlinear Wave Equations* (New York: Academic)
[13] Newell A C 1985 *Solitons in Mathematics and Physics* (Philadelphia, PA: SIAM)
[14] Agrawal G P 1989 *Nonlinear Fiber Optics* (Boston: Academic)
[15] Gagnon L and Winternitz P 1993 Symmetry classes of variable coefficient nonlinear Schrödinger equation *J. Phys. A: Math. Gen.* **26** 7061
[16] Gagnon L 1993 Soliton on a cw background and collosion between two dark pulses: some analytical results *J. Opt. Soc. Am.* B **10** 469
[17] Tomlinson W J, Stolen R H and Johnson A M 1985 Optical wave breaking of pulses in nonlinear optical fibers *Opt. Lett.* **10** 457
[18] Rothenberg J E 1989 Femtosecond optical shocks and wave breaking in fiber propagation *J. Opt. Soc. Am.* B **6** 2392
[19] Rasmussen J J and Rypdal K 1986 Blow-up in nonlinear Schrödinger equations–I: a general review *Phys. Scr.* **33** 481
[20] Rypdal K and Rasmussen J J 1986 Blow-up in nonlinear Schrödinger equations–II: similarity structure of the blow-up singularity *Phys. Scr.* **33** 498
[21] Le Mesurier B, Papanicolaou G, Sulem G and Sulem P 1988 Local structure of the self-focusing singularity of the nonlinear Schrödinger equation *Physica* **32D** 210
[22] Gagnon L and Stiévenart N 1994 N-soliton interaction in optical fibers; the multiple pole case *Opt. Lett.* **19** 619
[23] Daubechies I 1988 Orthonormal bases of compactly supported wavelets *Commun. Pure Appl. Math.* **41** 906
[24] Mallat S 1989 Multiresolution approximation and wavelet orthonormal bases of L^2 *Trans. Am. Math. Soc.* **315** 69
[25] Meyer Y 1993 *Wavelets, Algorithms and Applications* (Philadelphia, PA: SIAM)
[26] Daubechies I 1992 *Ten Lectures on Wavelets* (Philadelphia, PA: SIAM)
[27] Fleck J A, Morris J R and Feit M D 1976 Time-dependent propagation of high energy laser beams through the atmosphere *Appl. Phys.* **10** 129
[28] Lax M, Batteh J H and Agrawal G P 1981 Channelling of intense electromagnetic beams *J. Appl. Phys.* **52** 109
[29] See remark 2 in [26] p 253
[30] Beylkin G, Coifman R and Rokhlin V 1991 Fast wavelet transforms and numerical algorithms I *Commun. Pure Appl. Math.* **44** 141
[31] Beylkin G 1992 On the representation of operators in bases of compactly supported wavelets *SIAM J. Num. Anal.* **29** 1716
[32] Gagnon L, Lina J M and Goulard B 1994 Application of complex Daubechies' wavelets to numerical simulation of a nonlinear signal propagation model *IEEE Proc. 7th SP Workshop on Stat. Sign. and Array Processing (Quebec)* pp 251–54
[33] Press W H, Flannery B P, Teukolsky S A and Vetterling W T 1988 *Numerical Recipes in C* (Cambridge: Cambridge University Press)
[34] Florjanczyk M and Gagnon L 1990 Exact solutions for a higher-order nonlinear Schrödinger equation *Phys. Rev.* A **41** 4478
[35] Gagnon L and Bélanger P A 1991 Adiabatic amplification of optical solitons *Phys. Rev.* A **43** 6187
[36] Meyer Y and Roques S (eds) 1993 *Progress in Wavelet Analysis and Applications* (Gif-sur-Yvette: Frontieres)